ADVANCED ENGINEERING MATERIALS

FULL PAPER

DOI: 10.1002/adem.201600225

Potential of Photocurrent Improvement in μc-Si:H Solar Cells with TCO Substrates Structured by Direct Laser Interference Patterning**

By *Marcos Soldera,* Kurt Taretto, Jana Berger* and *Andrés Fabián Lasagni*

Thin film solar cells based on weak absorbers like hydrogenated microcrystalline silicon (μc–Si:H) need an effective light management to maximize light absorption. In this work, the authors study numerically the light trapping capability of boron doped zinc oxide (ZnO:B)-coated substrates textured by direct laser interference patterning (DLIP). The geometric parameters of the simulated patterns are taken from measurements of DLIP processed samples with sine-like grooves. The results suggest that this technology is suitable to enhance the photocurrent by 15–35% of μc–Si:H solar cells deposited on ZnO:B using texture periods between 0.8 and 1.5 μm and a 2 μm active layer.

1. Introduction

Thin film silicon photovoltaic technology has very attractive features to become an alternative to the still expensive wafer-based solar cells. On the one hand, hydrogenated microcrystalline silicon (μc-Si:H) can be grown from the gas phase, which is a much less intensive process in terms of energy consumption than growing crystalline silicon ingots.[1–3] Moreover, depositing only a few micrometers of silicon and avoiding ingot sawing greatly reduce the costs associated to material usage and waste. On the other hand, thin film modules can be fabricated monolithically in the same production line of the silicon deposition process.[4]

However, microcrystalline silicon suffers from a very low absorption coefficient in the red and infra-red portion of the solar spectrum limiting the photocurrent of the solar cells.[5] Therefore, improving light absorption in solar cells based on this moderate absorber is of paramount importance to achieve high power conversion efficiencies. One of the main challenges in the electro-optical design of these solar cells is to maximize light absorption using light trapping techniques, while keeping the thickness of the absorber as thin as possible. Fulfilling this requirement facilitates the transport of the photogenerated carriers to the contacts enhancing the photocurrent, open circuit voltage, and efficiency.[6,7]

Light trapping is commonly achieved by texturing the front surface of the layer stack that makes up the cell.[8–10] When light encounters the structured layer, it scatters into multiple directions increasing its optical path inside the photoactive material. Additionally, if the texture consists in a periodic pattern whose period is on the order of the wavelength of incoming light, then light may be diffracted into several modes with different propagation angles that lengthen the optical path.[11,12] Several manufacturing techniques have been proposed and used to fabricate periodic as well as random textures to enhance light trapping in μc-Si:H solar cells. For instance random textures with root mean square roughness of up to 300 nm were obtained using wet etching of aluminum-doped zinc oxide (AZO),[13,14] micrometer sized pyramids were transferred from a plastic mold to a glass substrate using imprint and UV photolithography,[15] and

[*] *Dr. M. Soldera, Prof. Dr. K. Taretto*
PROBIEN, Dto. de Electrotecnia, CONICET, Fac. de Ingeniería, Univ. Nacional del Comahue, Buenos Aires 1400, 8300 Neuquen, Argentina
E-mail: marcos.soldera@fain.uncoma.edu.ar
Dr. J. Berger, Prof. Dr. A. F. Lasagni
Institute of Manufacturing Technology, Technische Universität Dresden, George-Bähr-Straße 3c, 01069 Dresden, Germany
Fraunhofer Institute for Material and Beam Technology, Winterbergstraße 28, 01277 Dresden, Germany

[**] *The authors would like to acknowledge Dr. Campa (University of Ljubljana) for providing optical constants of intrinsic and doped microcrystalline silicon. M.S. and K.T. would like to thank PROBIEN-CONICET and Universidad Nacional del Comahue for supporting this work. The work of A.L. was supported by the German Research Foundation (DFG), Excellence Initiative by the German federal and state governments to promote top-level research at German universities (Grant No.: F-003661-553-41A-1132104). J.B. acknowledges the ESF "Europäischen Sozialfond" under grant number 100111052 for financial support and the Bosch Solar Energy AG for fabrication of the ZnO:B-films. This work was also supported by the SUMA2 Network Project, 7th Framework Program of the European Commission (IRSES Project N° 318903).*

ADVANCED ENGINEERING MATERIALS

periodic pyramids[16] and honeycomb-like textures[17] with sub-wavelengths periods were fabricated by photolithography. Although these methods succeeded in enhancing light absorption and therefore the photocurrent of the solar cells, they require several processing steps to achieve the final structure, including the disposal of hazardous chemicals.

Direct laser interference patterning (DLIP) is a novel method to produce periodic 1D and 2D patterns on metals, plastics, and ceramics.[18–20] In this method, a high-power laser beam is split into two or more sub-beams that interfere on the surface of a sample. Depending on the available energy density, the material can be ablated or locally modified at the interference maxima positions, while the material at the minima positions remains nearly unaffected compared to the positions of maximum intensity. The texture geometry can be adjusted by changing the angle of the sub-beams, the number of simultaneous overlapping beams, the number of laser pulses, and their energy density.[21,22] Furthermore, because the shape of the interference pattern is directly transferred to the substrate, no masks or solvents are needed. This fabrication technology is fully scalable to industrial standards, can be integrated into roll-to-roll facilities, and has processing speeds of about 1 $m^2\,min^{-1}$.[23] Recently, DLIP was used to successfully produce sine-like and hexagonal periodic patterns on transparent conductive oxides (TCO).[24–26]

In this work, we calculate the potential improvement in the photocurrent delivered by state-of-the-art μc-Si:H solar cells deposited on DLIP-patterned boron-doped zinc oxide (ZnO:B) coated substrates. Maxwell's equations are solved rigorously using finite element methods (FEM) to estimate the light absorption and photocurrent of texture shapes with real geometric parameters achievable with current DLIP technology according to our recent results. We also compare the performance of the solar cells deposited on textured substrates with equivalent solar cells with perfectly flat interfaces and also with equivalent devices deposited on native rough ZnO:B-coated substrates.

The outline of this work is described as follows. In Section 2, we present our recent experimental results concerning DLIP patterning of TCO substrates for applications in optoelectronic devices. Next, Section 3 describes the electromagnetic model developed in this work to obtain the photocurrent in solar cells. In Section 4, we show and discuss the most important results we obtain from the model and interpret the technological relevance of the simulations. Finally, in Section 5 we draw the conclusions and suggest an outlook for future improvements.

2. DLIP Processing of TCO-Coated Substrates

The processed samples consist of boron-doped zinc oxide (ZnO:B) films deposited on soda-lime glass substrates using low-pressure chemical vapor deposition. The as-deposited film has a thickness of 1.5 μm with a polycrystalline morphology, formed with large columnar monocrystalline grains, leading to surface pyramidal shape features.

Textured TCO substrates for applications as front electrodes on optoelectronic devices were made using a DLIP system based on a Nd:YAG laser (Quanta Ray Pro 290-10, Spectra-Physics) with a pulse duration of 8 ns. Since the ZnO:B has a high absorption coefficient in the UV, the laser was used in the 3rd harmonic at a wavelength 355 nm.[27,28]

The primary laser beam was split into two beams with the same intensity, which were then overlapped on the sample using mirrors. Given the different optical path length, an interference pattern was obtained. With this geometric setup, one-dimensional line-like patterns were formed. Additional information about the experimental setup can be found elsewhere.[18,20,29]

For the two-beam configuration, the spatial period p of the pattern is defined by the laser wavelength λ and the angle of incidence θ of the laser beams according to the following:

$$p = \frac{\lambda}{2\sin(\theta)} \tag{1}$$

To fabricate the periodic structures on large areas, a rectangular ceramic mask ($5 \times 7\ mm^2$) was used to change the shape of the incident beams into a rectangular beam. The samples were then mounted on an XYZ-motion system to scan the sample area. The total processed area was $50 \times 50\ mm^2$ for each produced structure.

Figure 1 shows representative profiles of patterns produced on ZnO:B-coated substrates. The spatial period of the produced patterns was i) 0.8, ii) 1.5, and iii) 5.0 μm, corresponding to overlapping angles of 12.7°, 6.8°, and 2.0°, respectively. The height of the produced structures was 82 ± 21, 221 ± 43, and 201 ± 32 nm for 0.8, 1.5, and 5.0 μm periods, respectively.

Previous investigations have shown that both the laser energy density (laser fluence) and the spatial period have a strong influence on the structure height.[26] In the case of

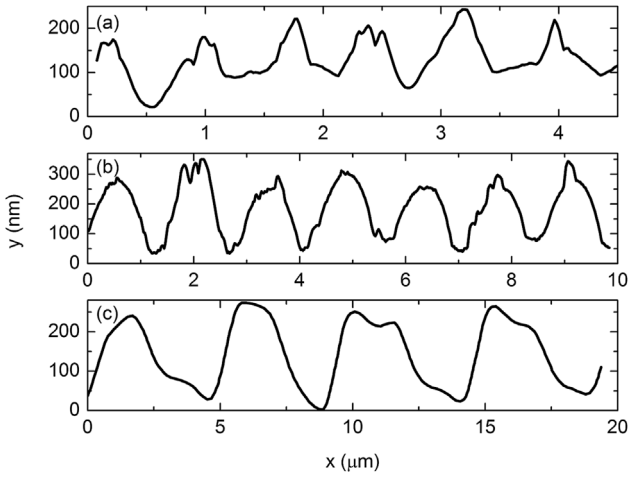

Fig. 1. Profiles of DLIP-processed ZnO:B-coated substrates with (a) one laser pulse with a fluence of 200 mJ cm^{-2} and spatial period of 800 nm, (b) three laser pulses with total fluence of 300 mJ cm^{-2} and period 1.5 μm, and (c) one pulse of 400 mJ cm^{-2} and a period of 5 μm.

ZnO:B-coated substrates, structure heights up to ≈250 nm are possible for spatial periods larger than 1.5 μm, using one laser pulse. These patterns can be obtained at laser energy densities (laser fluence) between 300 and 400 mJ cm^{-2}. For periodic structures with spatial periods in the sub-micron range (e.g., 0.8 μm), the maximal achievable structure height was ≈100 nm. A possibility to improve the resolution limit of the method as well as to produce structures with a higher aspect ratio is by using picosecond pulsed laser systems. In this way, thermal effects can be reduced permitting a higher thermal contrast between the maxima and minima positions.

3. Optical Model

We calculate the solar radiation absorption and photocurrent of hydrogenated microcrystalline silicon solar cells solving Maxwell's equations by the FEM. The solution takes into account diffraction and interference of incoming light between the layers interfaces in a two-dimensional simulation domain. Since we are seeking the steady state solutions of the problem, we follow the time harmonic propagation approach,[30] by which we assume that all variations in time can be expressed as sinusoidal signals. Then, setting the wavelength λ as a predefined variable, the obtained solutions are complex values that represent the amplitude and phase of the electric and magnetic field.

The simulated solar cell is based on the thin film silicon device studied in Čampa et al.[31] and described in Figure 2. It consists of a pin-type solar cell with an intrinsic μc-Si:H enclosed by thin p- and n-doped μc-Si:H layers deposited on a boron-doped zinc oxide (ZnO:B) coated soda-lime glass. Then, the silicon layers are capped with a ZnO buffer and an Ag contact. We model three geometric schemes representing different states of the DLIP processing. Namely, our starting point and reference device is that based on perfectly flat layers. Then, we simulate the solar cells grown onto native rough ZnO:B front electrode with an arithmetic roughness of 54.6 nm and a root mean square roughness of 67.6 nm, according to atomic force microscopy (AFM) measurements. It is expected that this rough surface scatters incoming light and therefore contributes to light trapping within the intrinsic silicon layer. To study this effect, we simulate solar cells prepared on rough ZnO:B-coated substrates using profiles extracted from AFM measurements. The five simulated profiles are shown in Figure 3, with their statistical magnitudes of interest. Finally, we simulate the engineered sine-like structures by DLIP with realistic geometries obtained from previous experimental results on ZnO:B or equivalent TCOs.[24,26] The geometric parameters used in the simulations are the period of the textures, which is swept between 0.8 and 5 μm, and the structure depth, varied between 100 and 500 nm. The combination of these parameters yields aspect ratios lying in the range 0.02 and 0.63. In all cases, we assume that the layers are grown conformally onto the front electrode.

The studied solar spectrum matches the standard AM1.5G bounded between 350 and 1100 nm since for shorter wavelengths light is strongly absorbed in the glass substrate and for wavelengths beyond 1100 nm the absorbance in the silicon layer can be neglected. The incoming solar radiation is assumed to be non-polarized.[32] This is accounted for by assuming that the solar spectrum is split into two components with the same electromagnetic power with, on the one hand, the electric field perpendicular to the plane of incidence (transverse electric case, TE), and on the other hand, the electric field parallel to the plane of incidence (transverse magnetic case, TM). The solutions obtained in each polarization mode are then averaged.

Since soda-lime glass substrates have a thickness of a few millimeters, we must handle solar light propagation incoherently in this domain. We deal with this issue by uncoupling light propagation within the substrate from the rest of the solar cell, where light is treated coherently. The incoming light enters from an inner virtual boundary between the soda-lime

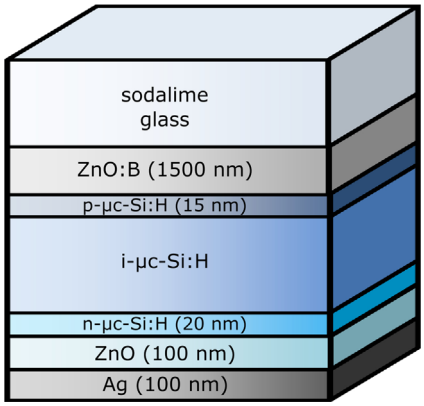

Fig. 2. Layer stack of the simulated solar cells.

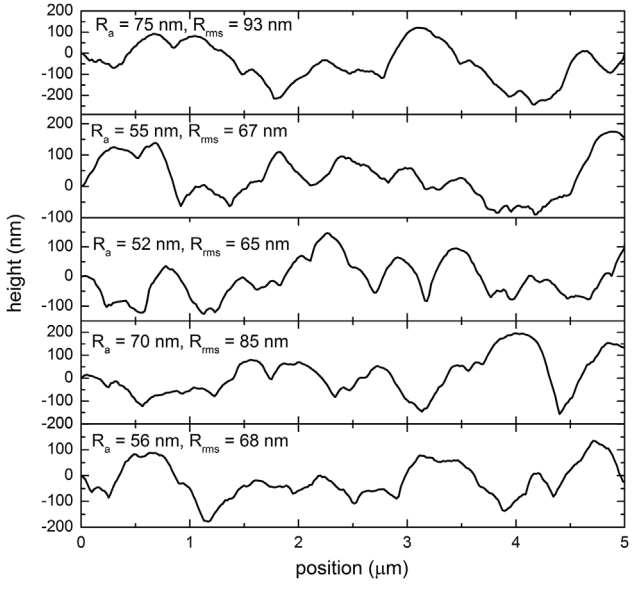

Fig. 3. Simulated profiles extracted from AFM measurements of native ZnO:B-coated soda-lime glass with their corresponding arithmetic roughness R_a and root mean square roughness R_{rms}.

glass substrate and the front electrode with an electromagnetic power reduced by the reflectance R_{glass} at the front surface

$$P_{incoherent}(\lambda) = \left(1 - R_{glass}(\lambda)\right) P_{AM15G}(\lambda) = \left(1 - \left(\frac{n_0 - n_{glass}}{n_0 + n_{glass}}\right)^2\right) P_{AM15G}(\lambda), \quad (2)$$

where $n_0 = 1$ and n_{glass} are the refractive index of air and soda-lime glass, respectively, and PAM15G is the wavelength-dependent solar power according to the AM1.5G standard. The global reflection will then be estimated as the sum between the front reflectance R_{glass} and the reflected light by the layer stack.

On top of the glass-front electrode interface, a perfectly matched layer (PML) with the same refractive index as soda-lime glass behaves as a semi-infinite absorbing medium to avoid subsequent re-entering of spurious reflected light.[33] The lateral boundary conditions are assumed to be periodic to account for diffraction of incoming light.

To obtain the photocurrent delivered by the solar cells, we first define the average electromagnetic energy density absorbed in a material with complex index of refraction $\tilde{n}(\lambda) = n(\lambda) + i\kappa(\lambda)$ as follows:[34]

$$Q(x, y, \lambda) = \frac{1}{2} c\varepsilon_0 n(\lambda)\alpha(\lambda)\left|\vec{E}(x, y, \lambda)\right|^2, \quad (3)$$

where λ is the free space wavelength of the plane electromagnetic wave, E is the electric field vector, c is the speed of light in vacuum, ε_0 is the permittivity of free space, and α is the absorption coefficient defined as $\alpha = 4\pi\kappa(\lambda)/\lambda$.

We assume that in the intrinsic silicon (i-Si) layer a free electron–hole pair is created per each absorbed photon, and neglect the contribution of photocarriers generated in the much thinner n- and p-doped layers. With the average electromagnetic energy absorbed in the intrinsic silicon layer $Q_{i\text{-}Si}$, we obtain the free carrier generation rate as follows:

$$G(x, y, \lambda) = Q_{i-Si}(x, y, \lambda)/(hc/\lambda), \quad (4)$$

where h is Planck's constant. Finally, in short circuit conditions we consider that every photogenerated carrier is extracted through the contacts of the solar cell. This implies that the maximum photocurrent density is given by integrating the generation rate in the volume and in the analyzed wavelength range, according to the following:

$$J_{photo} = q \int_{350\,nm}^{1100\,nm} \int_V G\, dV\, d\lambda/A, \quad (5)$$

where q is the elementary charge and A is the projected solar cell area in the substrate plane.

The electromagnetic model is implemented using the software COMSOL Multiphysics. For a detailed description of the electromagnetic model and its implementation in COMSOL see Soldera et al.[35] The mesh is generated by COMSOL using triangular elements with the constraint that the minimum effective wavelength exceeds at least five times the element size in each subdomain.[30] With this consideration, typical mesh sizes range from 80 000 to 150 000 elements.

4. Results and Discussion

Figure 4 shows the electric field norm for TE-polarized light at a wavelength of 700 nm in the simulated solar cells with 1 μm thick silicon deposited on i) perfectly flat substrate, ii) native rough ZnO:B (bottom profile of Figure 3), and iii) DLIP-processed substrate with depth $d = 500$ nm and period $p = 1.5$ μm. Figure 4a also shows the interior boundary from which light (arrows) enters the simulation domain, and the PML where all the reflected light is absorbed, mimicking a semi-infinite domain. Naturally, in the flat cell the electric field distribution is uniform in the x (horizontal) direction, while in the y (vertical) direction the distance between the peaks depends on the wavelength in each medium. Figure 4b confirms that the rough ZnO:B surface scatters light randomly, and therefore works as a light trapping scheme. The solar cell with the sine-like texture (Figure 4c) exhibits a symmetric distribution of the electric field, with its absolute maximum near the valley of the TCO due to the interference between the incoming light, the reflected, and diffracted light.

Figure 5 shows the simulated maximum photocurrent delivered by the solar cells for three different silicon thicknesses, i.e., i) 500 nm, ii) 1 μm, and iii) 2 μm. The symbols represent the devices with sine-like structures as a function of the period and the structure depth d as parameter. These figures also show as a reference the corresponding photocurrent calculated for the solar cells with perfectly flat interfaces (black-dashed line) and also the averaged photocurrent for the cells deposited on the five rough ZnO:B front electrodes as described earlier (blue dashed-dotted line). In all cases, we observe that the rough ZnO:B-coated substrates enhance the photocurrent relative to the flat device by scattering light randomly and thus promoting light trapping in the solar cell. The impact of this effect is more pronounced as the silicon thickness decreases, with the maximum relative increase in the photocurrent of 17% for a silicon thickness of 500 nm.

The simulations show that DLIP-patterned structures with periods smaller than 3 μm enhance the photocurrent of the solar cells compared to those devices based on flat and rough substrates. We observe that the shorter the period and the deeper the structures, the larger is the enhancement in the photocurrent. The 100 nm deep sinusoidal structures with a period of 0.8 μm provide an increase in the photocurrent between 13 and 19% compared to the flat device, while the structures with a depth of 500 nm could yield an enhancement of up to 31% for the same period.

Our findings are comparable to simulations using rigorous methods done previously on periodic patterned μc-Si:H

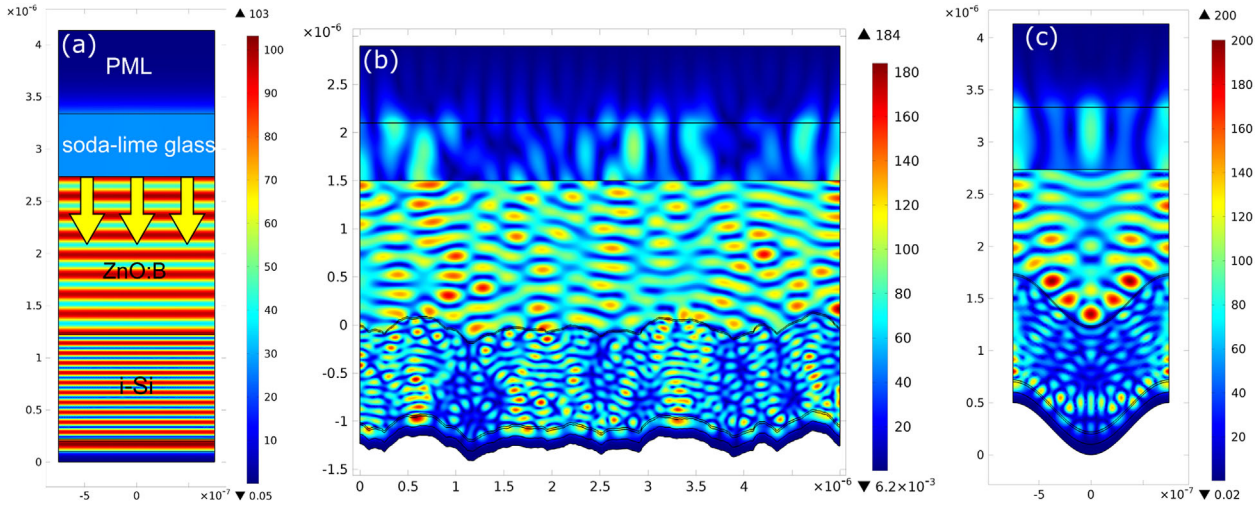

Fig. 4. Simulated electric field norm for TE-polarized light at a wavelength of 700 nm within solar cells with 1 μm thick silicon deposited on a perfectly flat substrate (a), on native rough ZnO:B (b), and on a DLIP-patterned substrate with depth $d = 500$ nm and period $p = 1.5$ μm (c).

solar cells. For instance Haase and Stiebig[36] used the finite integration technique (FIT) to find a photocurrent increase of 23 and 9% for rectangular periodic textures with period $p = 0.7$ μm and depth $d = 330$ nm, and $p = 1.5$ μm and $d = 200$ nm, respectively. Using the finite difference time domain method (FDTD), Dewan et al.[37] simulated triangular periodic patterned devices and obtained an enhancement in the photocurrent of 29 and 25% with parameters $p = 0.8$ μm and $d = 200$ nm, and $p = 1.5$ μm and $d = 200$ nm, respectively. Lastly, Campa et al.[31] used the FEM to model sine-like patterns and obtain an increase of 29 and 26% for textures with $p = 0.8$ μm and depth $d = 150$ nm, and $p = 1.5$ μm and $d = 300$ nm, respectively.

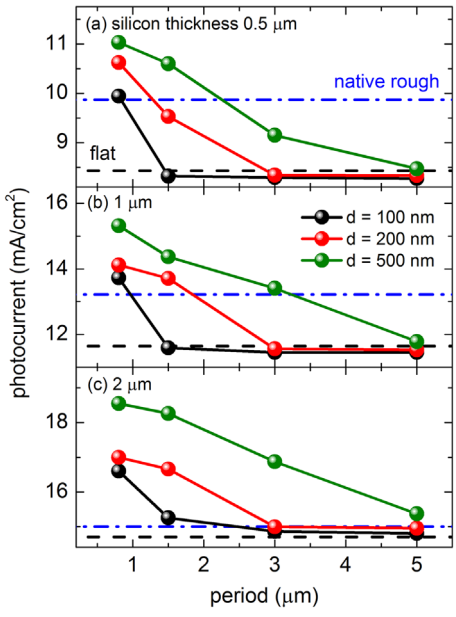

Fig. 5. Simulated photocurrent of solar cells with an absorber thickness of (a) 0.5 μm, (b) 1 μm, and (c) 2 μm on DLIP-processed substrates (spheres), on native rough substrates (blue dash-dotted line) and on perfectly flat substrates (black-dashed line).

The increase in the photocurrent upon structuring the substrate can be explained by three effects, which are schematically described in Figure 6: i) refraction of incoming light at the oblique ZnO:B/silicon interface changes the propagation angle of light yielding an increase in the optical path. This effect is present for all periods, but its effect is more pronounced for the shorter periods because at fixed structure depth the grooves have steeper angles. ii) Deep structures increase the probability that incoming rays that are reflected by the patterned TCO hit an adjacent facet of the texture and be refracted toward the silicon. Namely, light trapping takes place through multiple reflections between the structures that greatly increase the probability of light absorption in the silicon layer. This effect is more evident for structures with high aspect ratios, while it is disregarded for aspect ratios lower than 0.3.[38,39] iii) Diffraction of light by the periodic pattern promotes coupling of incoming light into several modes that propagate at oblique angles, increasing the optical path and light absorption in silicon. The diffraction efficiency

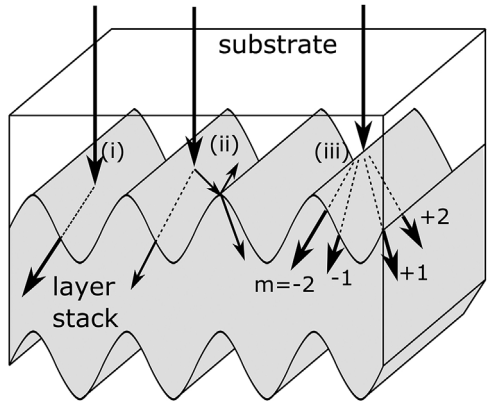

Fig. 6. Schematic representation of the optical mechanisms that contribute to light trapping upon DLIP processing of substrates. (i) Refraction and subsequent propagation at oblique angle, (ii) multiple reflections between adjacent facets, and (iii) diffraction of incoming light into multiple modes.

ADVANCED ENGINEERING MATERIALS

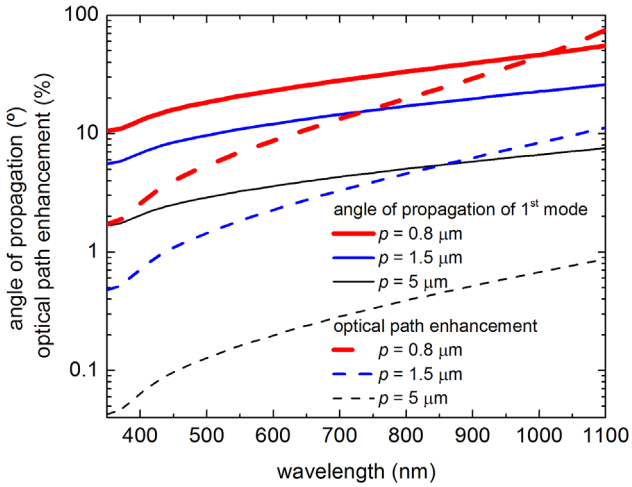

Fig. 7. Angle of propagation of the first-order diffracted mode of the patterned ZnO:B-coated substrate.

depends not only on the effective wavelength and grating period, but also on the structure's shape and depth. The well-known diffraction grating equation $(\sin(\theta_m) = m\lambda/p)$ states that the lower the period-to-effective wavelength ratio, the larger the angle of propagation θ_m of the mth diffracted mode. Figure 7 shows the angles of propagation of the first-order diffraction mode for three simulated periods at normal incidence and the corresponding relative increase in the optical path. The impact of the grating is more pronounced in the infrared portion of spectrum, where the absorption of silicon is weaker. At a period $p = 5\,\mu m$ the diffraction modes propagate at angles lower than 10°, and therefore the increase in optical path can be neglected.

To gain a deeper insight into the diffraction efficiency of these sine-like gratings, we model the patterned ZnO:B-coated substrates produced by DLIP working as diffraction gratings. Using the finite element method, we model a single slab of the periodic texture and define input and output ports to calculate the power flow of the different diffraction modes released by the grating at normal incidence. The lateral boundary conditions are set as periodic Floquet-type. The transmittance of the direct (zero-order), first- and second-order beams, the absorbance of the ZnO:B layer, and the total scattering, namely the sum of the first (±1) and second (±2) order modes transmittance, are shown in Figure 8a of a textured substrate with period $p = 1.5\,\mu m$ and depth $d = 200\,nm$, and in Figure 8b of a substrate with the same period and $d = 500\,nm$. We also show in Figure 8a the measured 1 st and 2nd diffracted orders, the total scattering, and the direct beam (stars) of a diffraction grating fabricated with DLIP with 1.5 μm period and groove depth of 190 nm. The samples were illuminated using a laser at a wavelength of 633 nm and the transmitted light was measured with a power meter.[26] The simulated grating with higher grooves, i.e., Figure 8b, shows a stronger scattering in the whole studied spectrum, which should explain the higher photocurrent obtained with this geometry. We observe that in the grating with $d = 500\,nm$, the first-order diffraction modes contribute on the total scattering mainly for wavelengths longer than 600 nm, while the second-order modes scatter light more strongly in the visible spectrum. Finally, notice that in Figure 8a the measured transmittance of the 1st diffraction mode correlates with the simulation, but the intensity of the 2nd order is seven times higher in the experiment than in simulation. This difference may arise from a non-homogeneous surface texture with small deviations in both period and depth, or overlapping periods by small melting bulges.

From the preceding discussion we conclude that, on the one hand, the patterns with $p > 3\,\mu m$, are not capable to trap light efficiently, nor increase the photocurrent, by none of the proposed optical mechanisms. However, if deeper structures with the same periods but aspect ratios higher than 0.3 could be patterned, then the mechanisms i) and ii) would start to play a role and enhance light trapping. On the other hand, the simulated textures with $p < 3\,\mu m$, increase absorption by taking advantage of the three proposed optical mechanisms. Our simulation tool does not let us to quantitatively

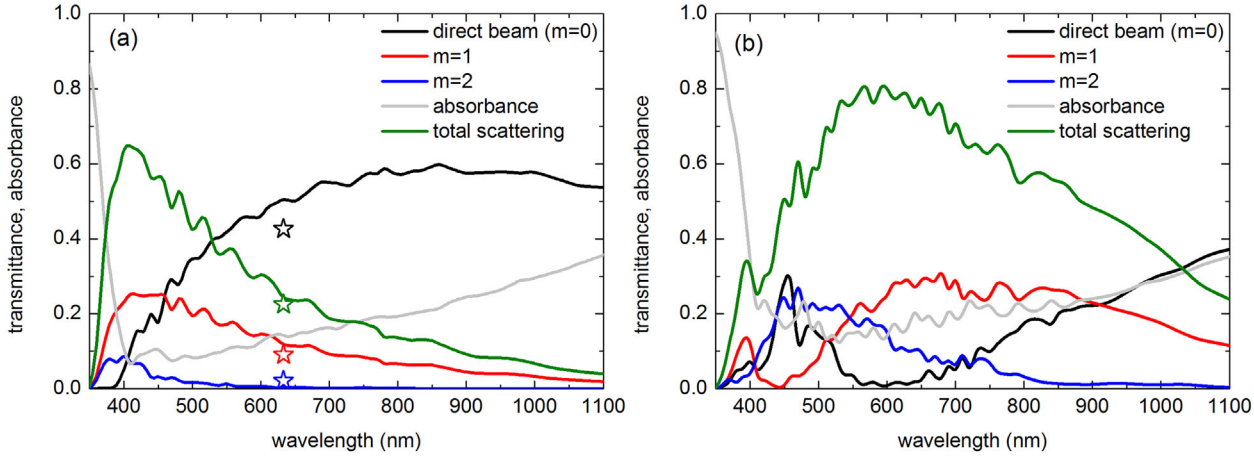

Fig. 8. Diffraction efficiency, absorbance, and scattering of simulated sine-like ZnO:B-coated soda-lime glass substrates with period $p = 1.5\,\mu m$ and depth (a) $d = 200\,nm$ and (b) $d = 500\,nm$. The stars in (a) represent the measurements on DLIP-processed samples illuminated with a laser at a wavelength of 633 nm.

determine the impact of each mechanism, although we estimate that diffraction should play a major role for those textures with periods $p < 1.5\,\mu m$ to increase the optical path inside the silicon layer.

When designing a solar cell, it is central to identify and quantify optical power losses to estimate the potential photocurrent loss associated to that design. The FEM allows us to calculate the power and photocurrent losses related to the absorbance of the contact layers and the global reflection. It is generally observed in our simulations that in the solar cells with pattern periods lower than $p < 3\,\mu m$, the increase in the absorbance in the active layer is correlated to a simultaneous decrease in the absorbance of the contact layers and in the global reflection. In order to illustrate this concept, we show in Figure 9a–d the absorbances in the active layer, in the ZnO:B, in the rest of the contact layers (which we call parasitic absorbance), and the reflectance, respectively, of the flat cell and the patterned cell with parameters $p = 0.8\,\mu m$ and $d = 500\,nm$. In both cells, the thickness of the silicon layer is 2 μm. It is worth noting that the ZnO:B coating is the contact layer that has by far the highest absorbance (roughly four times the sum of the rest of the contact layers). Although using DLIP a fraction of the ZnO:B material is removed, the optical path inside the ZnO:B coating is increased due to scattering and/or diffraction, compensating the reduction in thickness. Our calculations reveal that the photocurrent loss due to absorption in the ZnO:B layer is $J_{loss} = 12.54\,mA\,cm^{-2}$ in the flat cell and $J_{loss} = 11.57\,mA\,cm^{-2}$ in the patterned cell, representing 85 and 62% of the corresponding photocurrent, respectively. Bearing in mind that these photocurrent losses limit drastically the device efficiency, we simulate solar cells with a thinner ZnO:B layer, namely setting a thickness of 750 nm. The simulations yield a photocurrent of $J_{photo} = 16\,mA\,cm^{-2}$ with a photocurrent loss of $J_{loss} = 7.26\,mA\,cm^{-2}$ (45% of the photocurrent) for the flat cell and $J_{photo} = 20.8\,mA\,cm^{-2}$ and $J_{loss} = 5.55\,mA\,cm^{-2}$ (26% of the photocurrent) for the patterned device. Since the ZnO:B layer serves as a the front contact of the solar cell, there is a tradeoff between electrical and optical performance as a function of its thickness. Namely, the thinner the TCO layer, the larger the optical transmittance toward the silicon absorber, but the higher the electrical resistance and the ohmic losses. Therefore, we recognize that a careful optimization of the ZnO:B layer thickness taking into account both the electrical and optical losses should be addressed in order to maximize the power conversion efficiency of the solar cell.

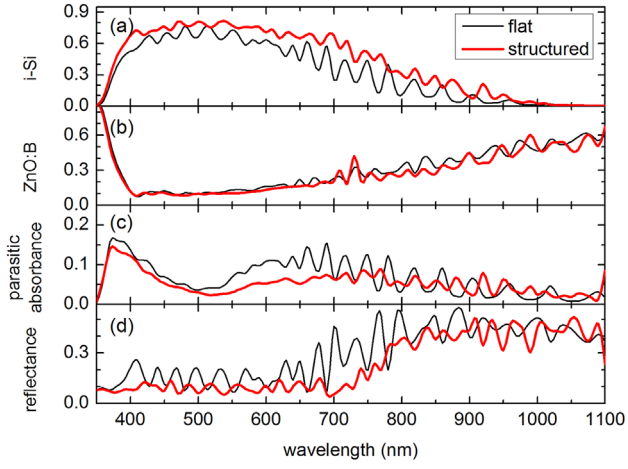

Fig. 9. Absorbance of the (a) intrinsic silicon, (b) ZnO:B coating, (c) rest of the contact layers other than ZnO:B, and (d) reflectance, of the flat solar cell and the structure device with period $p = 0.8\,\mu m$ and depth $d = 500\,nm$. In both cases, the silicon thickness is 2 μm.

On the other hand, the absorbances of the back contact layers of the patterned cell, i.e., n-Si, ZnO, and Ag, are approximately 50% lower compared to the flat cell since scattered light is now effectively absorbed in the intrinsic silicon. We also observe that upon structuring, the reflectance is strongly reduced in the whole spectrum up to 900 nm. The photocurrent loss due to reflection is then lowered from $12.81\,mA\,cm^{-2}$ in the flat cell to $9.92\,mA\,cm^{-2}$ in the patterned device. Despite this important reduction in the reflectance, we observe that there is still room for further reducing the reflectance in the infra-red spectrum, and thus increasing the absorbance in the active layer.

Summing up, the best performing solar cell simulated in this work has a pattern period $p = 0.8\,\mu m$ and depth $d = 500\,nm$, the silicon thickness is 2 μm and the front ZnO:B electrode is 750 nm thick. It delivers a photocurrent of $20.8\,mA\,cm^{-2}$, the reflectance represents a photocurrent loss of $9.92\,mA\,cm^{-2}$, while the current loss due to the absorbance in the TCO is $5.55\,mA\,cm^{-2}$, and due to the absorbance in the rest of the contact layers is $4.23\,mA\,cm^{-2}$. Analyzing the photocurrent losses, we are able to suggest further optimization steps toward a better light harvesting. On the one hand, texturing the front soda-lime glass surface with DLIP or another technique, for instance wet chemical etching, would reduce the front reflectance and further enhance the optical path. Another means to enhance the light incoupling to the solar cell could be the patterning of hierarchical textures on the ZnO:B layer with multiple periods using DLIP.[40,41] These structures combine the diffraction capability of the shorter pattern periods with the geometric light trapping through multiple reflections of the longer texture periods. On the other hand, optimization of the thickness of the ZnO:B layer should minimize its absorbance without compromising the electrical performance. We have found that the parasitic absorbances in the rest of the contact layers are rather small compared to values reported in the literature for similar devices.[42,43] However, additional simulations suggest that changing the buffer layer material (ZnO) by a more transparent material in the infra-red would further increase the photocurrent by roughly $1–2\,mA\,cm^{-2}$.

It is worth noting that a solar cell with perfectly flat interfaces would require a 5 μm silicon layer to deliver the same photocurrent of $20.8\,mA\,cm^{-2}$ like the best theoretical DLIP-patterned device with a 2 μm thick silicon layer. When using native rough ZnO:B-coated substrates, the silicon layer should be 4 μm to obtain the same photocurrent as the

optimized device. We then may conclude that patterning substrates with DLIP implies that the amount of silicon required to obtain the same device efficiency as an equivalent solar cell without any light trapping design is reduced by at least a factor 2.

It was recently reported that microcrystalline silicon grown on honeycomb-textured substrates develops cracks when the silicon thickness reaches a critical thickness which depends on the period and depth of the underlying texture.[44] Moreover, in this reference, an analytical model for crack prediction is presented and contrasted with experiments. Applying this model to our simulations, we were able to calculate that 1 μm thick μc-Si:H layer obtained by plasma-enhanced chemical vapor deposition would produce crack-free layers if textures with periods in the range $p = 0.8$–1.5 μm and depths up to $d = 200$ nm are used. In the case of preparing 2 μm thick μc-Si:H, crack-free layers would require periods $p > 1$ μm for a texture depth $d = 200$ nm and $p > 2$ μm for $d = 500$ nm. Comparing these results to our simulations (cf., Figure 5), we see that in general, the ranges of p and d that deliver the highest photocurrent improvements are not compromised by the potential crack formation model of ref.[44] It is important to point out that this model relies on honeycomb textures while our light trapping geometries are 1D sinusoidal gratings, which reduces the crack formation to only one direction, relaxing the conditions for crack formation estimated with the model of Tamang et al.[44]

5. Conclusions and Outlook

According to the 2D simulations presented in this work, solar cells fabricated on DLIP-patterned substrates with periods shorter than 3 μm should deliver a higher photocurrent than the untreated devices due to a better light management inside the cell. Our previous experimental results suggest that DLIP can be used to fabricate sine-like structures on boron-doped zinc oxide with a depth of 200 nm and a period of 1.5 μm as well as textures with depths of about 100 nm and a period of 800 nm. The simulation results indicate that these patterns have the potential to increase the photocurrent in the range 10–15% of μc-Si:H solar cells, compared to the flat devices.

We found that those solar cells with the thickest silicon layer, i.e., 2 μm, show the highest photocurrent and the highest relative photocurrent enhancement to their corresponding flat device. In particular, the solar cell textured with period $p = 1.5$ μm and depth $d = 200$ nm delivered a photocurrent of 16.7 mA cm^{-2}, which represents an enhancement of 14% relative to the flat device and of 11% relative to the native ZnO:B-based device.

We stress that patterns with depths beyond 400 nm and periods of about 1 μm, meaning aspect ratios up to 0.4, were already fabricated on 900 nm thick aluminum-doped zinc oxide (AZO) coated glass using DLIP.[24] Accordingly, we find that such structures on a 750 nm thick ZnO:B should be within reach using existing DLIP technology, which enable a photocurrent of 20.8 mA cm^{-2} in 2 μm thick solar cells, representing a promising relative enhancement of 35% compared to the flat case.

An important alternative application of the light trapping strategy presented here is that ZnO:B-coated substrate can be used as front electrode for other photovoltaic technologies, for instance for tandem microcrystalline/amorphous silicon tandem cells and for the disruptive technology of organo-metal halide perovskite-based solar cells.

We now describe briefly how the adding of a direct laser interference patterning step would impact on the cost of producing a microcrystalline silicon photovoltaic module. As reported in Lasagni et al.,[45] the manufacturing cost of the DLIP technology is approximately 3.08 € m^{-2} for processing TCO materials (calculation considering one operator working 52 weeks, 39 h a week with 100% overhead as well as cost necessary for purchasing the equipment distributed in 3 years at maximum achievable fabrication speed). Considering that a 6 × 6 in. thin film PV module has an area of 0.023 m^2, this represents a cost of 0.071 € per module. The price of a thin film module of this size is around 1.5–2.5 € Wp^{-1}. In consequence, the price increases only 2.8–4.7%. According to the reported results, an increase of the solar cell efficiency of 15% is possible. In consequence, the DLIP process reduces the €/Wp ratio about 8.9–10.6%. In addition, the manufacturing time for 1 m^2 is about 1–2 m^2 min^{-1}[45] representing in the worst case a processing time of 1.38 s per 6 × 6 in. module.

Article first published online: July 14, 2016
Manuscript Revised: June 16, 2016
Manuscript Received: April 26, 2016

[1] M. Konagai, *Jpn. J. Appl. Phys.* **2011**, *50*, 30001.
[2] S. Peng, D. Wang, F. Yang, Z. Wang, F. Ma, *J. Nanomater.* **2015**, *2015*, 88.
[3] C. Strobel, B. Leszczynska, U. Merkel, J. Kuske, D. D. Fischer, M. Albert, J. Holovský, S. Michard, J. W. Bartha, *Sol. Energy Mater. Sol. Cells* **2015**, *143*, 347.
[4] S. Haas, S. Krumscheid, A. Bauer, A. Lambertz, U. Rau, *Prog. Photovolt: Res. Appl.* **2013**, *21*, 972.
[5] A. Poruba, A. Fejfar, Z. Remeš, J. Špringer, M. Vaněček, J. Kočka, J. Meier, P. Torres, A. Shah, *J. Appl. Phys.* **2000**, *88*, 148.
[6] R. Brendel, *Thin-Film Crystalline Silicon Solar Cells*, Wiley-VCH, Weinheim, Germany **2003**, p. 11.
[7] F.-J. Haug, C. Ballif, *Energy Environ. Sci.* **2015**, *8*, 824.
[8] R. Brendel, D. Scholten, *Appl. Phys. A Mater. Sci. Process* **1999**, *69*, 201.
[9] J. A. Rand, P. A. Basore, Conf. Record of the Twenty Second IEEE, Las Vegas, NV, **1991**, 192.
[10] J. Springer, B. Rech, W. Reetz, J. Müller, M. Vanecek, *Sol. Energy Mater. Sol. Cells* **2005**, *85*, 1.
[11] C. Haase, H. Stiebig, *Appl. Phys. Lett.* **2007**, *91*, 61116.
[12] R. Dewan, D. Knipp, *J. Appl. Phys.* **2009**, *106*, 74901.

[13] G. Yang, R. A. Swaaij, O. Isabella, M. Zeman, *Prog. Photovolt: Res. Appl*. **2015**, *23*, 1283.
[14] M. Berginski, J. Hüpkes, M. Schulte, G. Schöpe, H. Stiebig, B. Rech, M. Wuttig, *J. Appl. Phys*. **2007**, *101*, 74903.
[15] J. Escarré, K. Söderström, M. Despeisse, S. Nicolay, C. Battaglia, G. Bugnon, L. Ding, F. Meillaud, F.-J. Haug, C. Ballif, *Sol. Energy Mater. Sol. Cells* **2012**, *98*, 185.
[16] H. L. Chen, K. T. Huang, C. H. Lin, W. Y. Wang, W. Fan, *Microelectron. Eng*. **2007**, *84*, 750.
[17] H. Sai, K. Maejima, T. Matsui, T. Koida, M. Kondo, S. Nakao, Y. Takeuchi, H. Katayama, I. Yoshida, *Jpn. J. Appl. Phys*. **2015**, *54*, 08KB05.
[18] M. D'Alessandria, A. Lasagni, F. Mücklich, *Appl. Surf. Sci*. **2008**, *255*, 3210.
[19] A. F. Lasagni, D. F. Acevedo, C. A. Barbero, F. Mücklich, *Adv. Eng. Mater*. **2007**, *9*, 99.
[20] J. Berger, M. Grosse Holthaus, N. Pistillo, T. Roch, K. Rezwan, A. F. Lasagni, *Appl. Surf. Sci*. **2011**, *257*, 3081.
[21] A. Lasagni, F. Mücklich, *Appl. Surf. Sci*. **2005**, *240*, 214.
[22] A. Lasagni, A. Manzoni, F. Mücklich, *Adv. Eng. Mater*. **2007**, *9*, 872.
[23] A. Lasagni, T. Roch, M. Bieda, D. Benke, E. Beyer, in *Proc. SPIE 8968, Laser-Based Micro- and Nanoprocessing VIII*, SPIE, San Francisco, United States **2014**, 89680A.
[24] S. Eckhardt, C. Sachse, A. F. Lasagni, *Phys. Procedia* **2013**, *41*, 552.
[25] S. Ring, S. Neubert, C. Schultz, S. S. Schmidt, F. Ruske, B. Stannowski, F. Fink, R. Schlatmann, *Phys. Status Solidi-R* **2015**, *9*, 36.
[26] J. Berger, T. Roch, S. Correia, J. Eberhardt, A. F. Lasagni, *Thin Solid Films* **2016**, *612*, 342.
[27] S. Faÿ, J. Steinhauser, S. Nicolay, C. Ballif, *Thin Solid Films* **2010**, *518*, 2961.
[28] M. K. Debanath, S. Karmakar, *Mater. Lett*. **2013**, *111*, 116.
[29] M. Bieda, E. Beyer, A. F. Lasagni, *J. Eng. Mater. Technol*. **2010**, *132*, 31015.
[30] COMSOL AB, *RF Module User's Guide*, **2008**.
[31] A. Čampa, J. Krč, M. Topič, *J. Appl. Phys*. **2009**, *105*, 83107.
[32] E. Lorenzo, in *Handbook of Photovoltaic Science and Engineering* (Eds: A. Luque, S. Hegedus), John Wiley & Sons, Ltd, West Sussex, United Kingdom **2010**, p. 984.
[33] J.-M. Jin, *The Finite Element Method in Electromagnetics*, John Wiley & Sons, Inc., New York **2002**, p. 371.
[34] L. A. A. Pettersson, L. S. Roman, O. Inganas, *J. Appl. Phys*. **1999**, *86*, 487.
[35] M. Soldera, E. Estrada, K. Taretto, *Phys. Status Solidi A* **2013**, *210*, 1345.
[36] C. Haase, H. Stiebig, *Prog. Photovolt: Res. Appl*. **2006**, *14*, 629.
[37] R. Dewan, M. Marinkovic, R. Noriega, S. Phadke, A. Salleo, D. Knipp, *Opt. Express* **2009**, *17*, 23058.
[38] S.-B. Rim, S. Zhao, S. R. Scully, M. D. McGehee, P. Peumans, *Appl. Phys. Lett*. **2007**, *91*, 243501.
[39] M. Soldera, E. Estrada, K. Taretto, *MRS Proc. Symp. E/H – Photovoltaic Technologies, Devices and Systems Based on Inorganic Materials, Small Organic Molecules and Hybrids*. Cambridge University Press, Cambridge, United Kingdom **2013**, 317.
[40] A. F. Lasagni, P. Shao, J. L. Hendricks, C. M. Shaw, D. C. Martin, S. Das, *Appl. Surf. Sci*. **2010**, *256*, 1708.
[41] M. Steger, C. Hartmann, S. Beckemper, J. Holtkamp, A. Gillner, *J. Laser Micro. Nanoeng*. **2013**, *8*, 210.
[42] R. Dewan, I. Vasilev, V. Jovanov, D. Knipp, *J. Appl. Phys*. **2011**, *110*, 13101.
[43] T. Lanz, B. Ruhstaller, C. Battaglia, C. Ballif, *J. Appl. Phys*. **2011**, *110*, 33111.
[44] A. Tamang, H. Sai, V. Jovanov, S. I. Bali, K. Matsubara, D. Knipp, *Sol. Energy Mater. Sol. Cells* **2016**, *151*, 81.
[45] A. F. Lasagni, T. Roch, J. Berger, T. Kunze, V. Lang, E. Beyer, *Proc. SPIE 9351, Laser-Based Micro- and Nanoprocessing IX*, SPIE, San Francisco, United States **2015**, 935115.

